Eur. Phys. J. B **50**, 371–378 (2006)
DOI: 10.1140/epjb/e2006-00157-2

THE EUROPEAN PHYSICAL JOURNAL B

Modeling the emission red-shift in amorphous semiconductors and in organic-inorganic hybrids using extended multiple trapping

R.A. Sá Ferreira[1,2], A.L. Ferreira[1], and L.D. Carlos[1,2,a]

[1] Departamento de Física, Universidade de Aveiro, 3810–193 Aveiro, Portugal
[2] CICECO, Universidade de Aveiro, 3810–193 Aveiro, Portugal

Received 27 October 2005 / Received in final form 6 December 2005
Published online 5 May 2006 –

Abstract. A model of thermal relaxation within localized states based on the extended multiple trapping framework is used to describe the red-shift of the emission maximum intensity as the excitation energy decreases. The model is applied to amorphous hydrogenated silicon (a-Si:H) and to organic-inorganic hybrids systems giving values for the energy gap, E_0, (1.896–3.882 eV) and for the β (4.36–12.08 eV^{-1}) parameter that characterizes the experimental decay of the density of localized states within the gap consistent with those achieved by some other recombination models previously reported for a-Si:H.. The thermal relaxation within localized states model is more physically detailed incorporating radiative and non-radiative transition mechanism for carriers relaxing into localized states that are explicitly absent in the previously reported theoretical descriptions

PACS. 78.55.Qr Amorphous materials; glasses and other disordered solids – 81.05.Gc Amorphous semiconductors – 81.07.Pr Organic-inorganic hybrid nanostructures

1 Introduction

The lack of long-range order characteristic of amorphous semiconductors, a-SC, is the main factor that determines their singular photoluminescence properties, that are not observed in crystalline semiconductors [1,2]. In particular, we can refer the red-shift of the emission energy as the excitation energy decreases. Transport and photoluminescence properties are determined by the disorder effects in the density of states, namely the inclusion of localized states within the forbidden optical gap characteristic of crystalline structures [1]. In particular, photoluminescence has been attributed to the recombination of electrons and holes separately trapped in such band tail states [1(b),2]. High energy carriers excited in extended states thermalize rapidly to the bottom of the bands where further thermalization into localized states proceeds much slowly and in competition with recombination processes.

Although several reports have been produced showing the excitation energy dependence of the light emission for different a-SC, such as amorphous hydrogenated silicon, a-Si:H [2–7], chalcogenide glasses, namely, As_2Se_3 [8], hydrogenated amorphous carbon [9–11], alloys of silicon and hydrogen carbon [12], porous silicon [13] and siloxene, $Si_6(OH)_3H_3$ [14], the physical mechanisms behind it are still controversial. That emission red-shift is also observed in efficient white-light photoluminescent organic-inorganic hybrids lacking metal activator ions, such as those obtained from 3-aminopropyltriethoxysilane (APTES) [15] and from urea cross-linked xerogels, classed as di-ureasils [16–21].

The concept of "hybrid organic-inorganic" materials emerged in the last two decades with the birth of "soft" inorganic chemistry processes (essentially the sol-gel method) [22]. In addition to the high versatility in chemical and physical properties and in shaping and patterning, hybrid materials present the crucial advantage to facilitate both integration and miniaturization. Therefore, a significant number of innovative and advanced hybrids have been synthesized in the past few years opening a land of promising applications in many fields: optics, electronics, ionics, mechanics, membranes, functional and protective coatings, catalysis, sensors, biology, medicine, biotechnology, etc. [23].

The emission energy dependence with changes in the excitation energy has been extensively studied for the case of amorphous hydrogenated silicon a-Si:H [3–7]. The radiative transitions involving carriers excited into localized states as been proposed as responsible for the excitation energy dependence of the emission energy in amorphous semiconductors. Chen et al. proposed a thermalization gap model trying to reproduce quantitatively the experimental observations [3,4]. Boulitrop et al. proposed that the excited carriers thermalize within an exponential tail of localized states and that the radiative transitions occur

[a] e-mail: lcarlos@fis.ua.pt

within the lowest energy states among a given number N of available states [2].

In this work, we propose a new model — designated as thermal relaxation within localized states — that clarify the physical mechanisms behind the thermalization processes considering that the excited carriers can move within localized states accordingly to the extended multiple trapping approach [5,6]. Such approach was previously used to study the time-dependent emission of a-Si:H after a excitation pulse with energy well above the optical absorption edge for this system [6]. Starting from the extended multiple trapping model, we consider here more general conditions of excitation, namely the excitation with photons of arbitrary energy below the absorption edge. Under low intensity excitation conditions the time integrated emission intensity after a pulse excitation at $t = 0$ can be shown to be equivalent to the steady-state emission intensity under a continuous excitation of the system. For each excitation energy we computed the emission spectra which red-shifts as the excitation energy decreases. The carriers excitation is directly determined from the density of states considered and the number of involved states in the thermal relaxation is determined by the localization degree of the states and by the carriers lifetimes prior to emission. These quantities — degree of state localization and transition rates — give a dynamic interpretation to the recombination process, which is somewhat hidden in previous descriptions of the red-shift phenomena.

This model is tested for a-Si:H, the results obtained are consistent with those achieved by previously reported recombination models, and it is applied to two sol-gel derived organic-inorganic di-ureasils hybrids. The thermal relaxation within localized states model is thereby suitable to describe quantitatively the recombinations mechanisms subjacent to the emission red shift as the excitation energy decreases. Moreover, time-dependent and steady-state results can be simultaneously considered.

2 Experimental emission red-shift data

The red-shift of the emission energy (E_p) as the excitation energy (E_x) decreases has been reported for several a-SC materials. In particular, we can refer different samples of a-Si:H investigated by several groups [2–7] and a-C:H prepared from toluene and benzene [9]. For a-Si:H, the emission peak position varies from 1.26 to 1.38 eV, for excitation energies between 1.55 and 1.83 eV [3,4]. This variation is linear and has a E_p/E_x slope around 0.5 [3]. For excitation energies between 2.97 and 3.60 eV (2.26 and 2.77 eV) the emission energy of the a-C:H films prepared from toluene (benzene) present a linear regime with a slope around 0.22 (0.44), and the energy peak position changes from 2.61 to 2.77 eV (2.07 to 2.19 eV) [9]. Increasing the excitation energy beyond these values the emission energy remains approximately constant [9].

Through the analyses of the data available in the literature, we collected the energy peak position versus the corresponding excitation energy for some

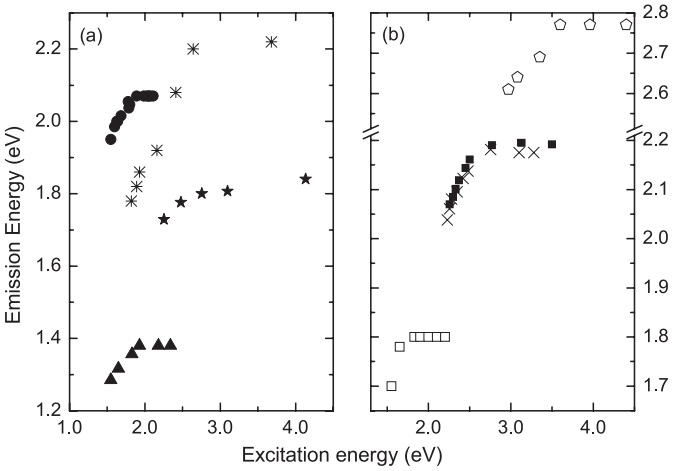

Fig. 1. Variation of E_p with E_x for different a-SC (a) a-Si:H (●,▲) [2–4], a-SiC:H [12] (∗), p-Si (★) [13], $Si_6(OH)_3H_3$ (▼) [14]; (b) As_2Se_3 (□) [8], a-C:H_D (X) [11], a-C:H prepared from toluene (⬠) and benzene (■) [9].

a-SC, As_2Se_3 [8], a-C:H [10], hydrogenated carbon (diamond-like), a-C:H_D [11], a-SiC:H [12], p-Si [13], and $Si_6(OH)_3H_3$ [1]. The slope E_p/E_x is 0.50 ± 0.06 for As_2Se_3, a-C:H, and a-SiC:H and for the remaining samples ranges from 0.09 ± 0.03 (p-Si) to 0.41 ± 0.01 ($Si_6(OH)_3H_3$). Figure 1 assembles all these experimental results.

The red-shift of the emission energy as the excitation energy decreases has also been observed in organic-inorganic hybrids, such as di-ureasils. The di-ureasil organic-inorganic hybrids are formed by a siliceous network covalently bonded through urea linkages to oxyethylene polymer chains with two distinct average polymer repeat units (40.5 and 8.5, designated as d-U(2000) and d-U(600), respectively). The di-ureasils, prepared as detailed reported elsewhere [16,19,21], display an efficient white light photoluminescence in the temperature range between 14 and 300 K [16,18–21]. The emission maximum intensity peak, E_p, strongly depends on the excitation energy, E_x [16,18–21], as exemplified in Figure 2. The emission was acquired at 14 K using a 0.25 m KRATOS GM-252 excitation monocromator and a 1 m 1704 SPEX Czerny-Turner spectrometer coupled to an RCA C31034 photomultiplier. The excitation source was 1000 W xenon arc lamp coupled to a KRATOS LH 15 IN/1 S monochromator.

These emission features were already intensively studied either by steady-state and time-resolved spectroscopy [18–21]. Such studies allowed us to conclude that their emission results from the overlap of donor-acceptor pair recombinations occurring in the siliceous nanodomains and in the NH groups of the urea linkages [20,21]. For excitation energies between 3.10 and 3.76 eV (330–400 nm), the deconvolution fitting procedure revealed the presence of two Gaussian bands, in the blue and purplish-blue spectral regions, whereas for excitation wavelengths higher than 3.10 eV (400 nm) the emission spectra display only the blue component (inset in Fig. 2) [20,21]. For the excitation energy range

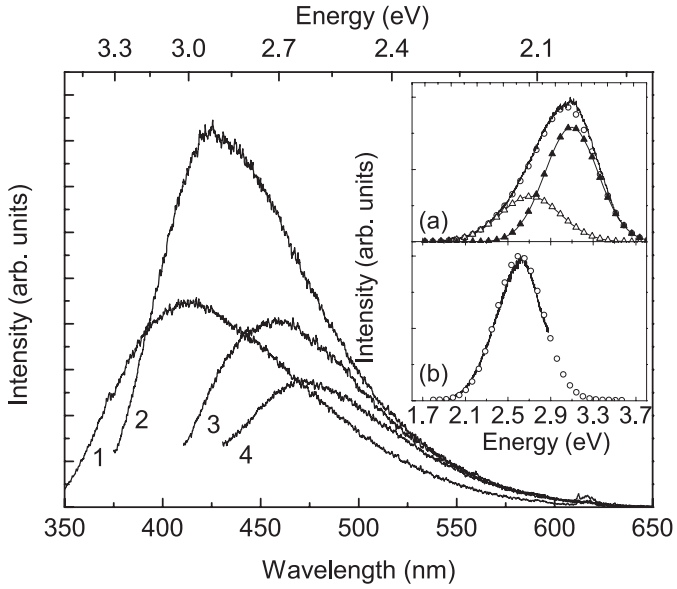

Fig. 2. Emission spectra (14 K) of the d-U(2000) di-ureasil under different excitation wavelengths: (1) 330 nm, (2) 365 nm, (3) 400 nm and (4) 420 nm. The insets show (a) the fitted Gaussian components, blue (open triangles) and purplish-blue (solid triangles), and the resulting overlap (◯) and (b) the blue band (◯) for the emission spectra exited under 365 and 420 nm, respectively.

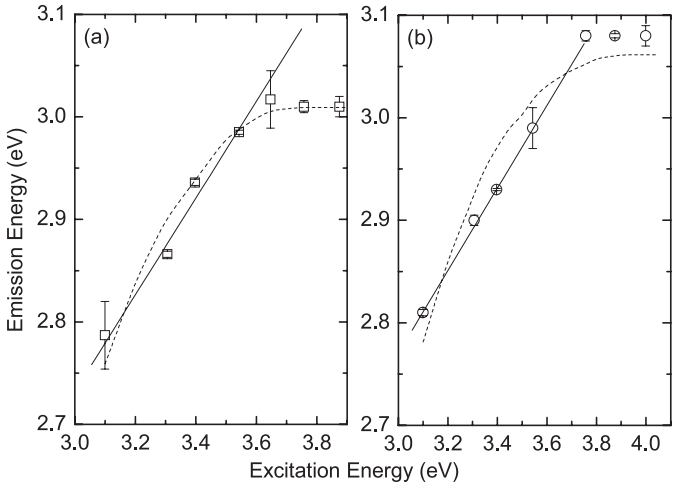

Fig. 3. Variation of E_{p} with E_{x} for (a) d-U(2000) and (b) d-U(600). The solid line represents the linear fit to the data ($R > 0.999$) within the linear region; and the dashed lines correspond to the same variation calculated by the thermal relaxation within localized states model.

used (2.95–3.76 eV), the energy of the blue band (related with the NH groups) is within 2.5–2.6 eV, whereas that of the purplish-blue band (associated with the siliceous nanodomains) varies between 2.7 and 3.0 eV. In that excitation energy interval is the purplish-blue band the responsible for the red-shift of the overall emission. Therefore, we will only take into account in the rest of the paper the emission features of that siliceous nanodomains-related component.

In Figures 3a, 3b we represent the dependence of the purplish-blue emission energy on the excitation energy for d-U(2000) and d-U(600), respectively. The variation of E_{p} with the increase of E_{x} presents two distinct regimes: (i) linear regime, characterized by a slope $E_{\mathrm{p}}/E_{\mathrm{x}}$ around 0.5 and (ii) saturation regime, in which the emission peak position is independent of the excitation energy [20,21]. This behavior is also common to other classes of organic-inorganic hybrids, namely APTES-derived materials and urethane cross-linked xerogels designated as di-urethanesils [21]. In all cases small changes are detected in the emission energy (<0.5 eV) and the slope $E_{\mathrm{p}}/E_{\mathrm{x}}$ remains approximately equal to 0.5 [21].

3 Numerical modelling

3.1 Thermalization gap model

The thermalization gap model was first suggested to explain the observed red-shift of the emission spectra of a-Si:H samples when the excitation energy was varied between 1.55 and 1.83 eV [3,4]. It was observed a linear dependence between the emission peak and the excitation energy with a slope approximately equal to 0.5 [3,4]. For excitation energies between 1.83 and 2.34 eV, the emission energy peaks at a constant value. In an attempt to explain such experimental results, Chen et al. [3] proposed the thermalization gap model, assuming that the conduction band is parabolic and that there is no density of states below the energetic minimum of the conduction band, E_{oc}. The valence band is described by an exponential function, and above the top of the valence band, E_{ov}, there is a density of localized states. In a qualitative way, this model stands that the holes created below E_{ov} thermalize to E_{ov} and that the electrons excited to the conduction band rapidly thermalize to the minimum of the band, E_{oc}, and recombine with a given energy E_{ot} [3,4]. This means that all the holes below E_{ov} generate an unshifted spectrum. However, if the excitation energy is smaller than $E_{\mathrm{o}} = E_{\mathrm{oc}} - E_{\mathrm{ov}}$, then there are holes with energy ΔE above E_{ov}, that recombine with electrons at E_{oc}, generating an identical emission spectrum to the one obtained in the previous situation but red shifted by an energy ΔE [3,4]. Chen et al. suggested that the emission intensity of the experimental spectra, $I(\hbar\omega)$, can be written as a sum of these two contributions [3]:

$$I(\hbar w) = N_{\mathrm{b}} I_0(\hbar w) + \int_{\max(E_{\mathrm{ov}}+E_{\mathrm{x}},E_{\mathrm{oc}})}^{E_{\mathrm{x}}+E_{\mathrm{F}}} \times I_0(\hbar w + \Delta E) g_{\mathrm{c}}(E) g_{\mathrm{v}}(E - E_{\mathrm{x}})\, dE \quad (1)$$

where $N_{\mathrm{b}} \propto \int_{E_{0\mathrm{c}}}^{E_{\mathrm{x}}+E_{0\mathrm{v}}} g_{\mathrm{c}}(E)\, g_v(E - E_{\mathrm{x}}) dE$ represents the number of holes below E_{ov} and E_{F} is the Fermi level. The first term $N_{\mathrm{b}} I_0(\hbar w)$ corresponds to the unshifted spectra weighted by the number of holes below E_{ov}. The second term expresses the emission intensity of the spectrum red shifted by ΔE, with respect to the previous case, and weighted by the convolution of the density of the involved

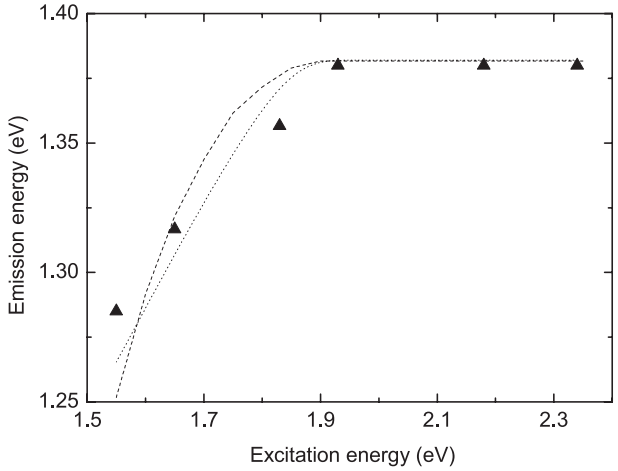

Fig. 4. Variation of E_p with E_x for a-Si:H [3,4]. The dashed and dotted lines correspond to the same variation calculated by the thermal relaxation within localized states model and the thermalization gap model, respectively.

states [3]. The integration variable E is the energy of the excited states in the conduction band. Consequently, the upper integration limit, $E_\mathrm{x} + E_\mathrm{F}$, corresponds to the higher energy level accessible to the electrons in the conduction band after excitation. The lower integration limit, $\max(E_\mathrm{ov} + E_\mathrm{x}, E_\mathrm{oc})$, is the lowest energetic value in the conduction band where it is possible to excite electrons (coming from electron states in the valence band with an energy larger than E_ov). The shift of the emission spectrum, $\Delta E = E - E_\mathrm{x} - E_\mathrm{ov}$, is the difference between the energy of the electron promoted from the valence band with an energy (E–E_x) and the limit of the thermalization gap, E_ov.

We have calculated $I(\hbar\omega)$ through equation (1) assuming that the emission spectra are well reproduced by a Gaussian function and using the parameters provided by references [3] and [4] for a-Si:H. We found that the linear dependence of E_p vs. E_x for excitation energies between 1.55 and 1.83 eV is described by a slope always equal to one. In spite of a nice qualitative description of the experimental results, namely the emission red shift with decreasing excitation energy, this model is not adequate to predict quantitatively the experimental $E_\mathrm{p}/E_\mathrm{x}$ slope (approximately 0.5). Figure 4 compares the experimental results reported for a-Si:H [3,4] with those estimated by the thermalization gap model.

3.2 Boulitrop et al. model

Boulitrop et al. proposed a different model in order to explain the red shift of the emission with decreasing excitation energy of a-Si:H [2]. This model, contrarily to the thermalization gap one, describes quantitatively the linear dependence observed between the emission (E_p) and the excitation energy (E_x). This model assumes that the optical excitation is induced by electron-hole pairs with an available exponential density of states given by:

$$g_\mathrm{L}(E) \propto \exp\left[-\beta_\mathrm{L}(E - E_0)\right]. \tag{2}$$

where E_0 is the band gap. This exponential density of states arises as a consequence of the fact that the density of states of electrons and holes has an exponential band tail characterized by the β_v and β_c parameters, respectively. It turns out that for $\beta_\mathrm{v} \sim \beta_\mathrm{c} \sim \beta$ we should have $\beta_\mathrm{L} \sim \beta/2$ [2].

The peculiarity of this model consists in considering that thermalization occurs to the lower energetic state among $N+1$ randomly chosen localized states, from which the emission occurs [2]. The probability, $P(E)$, to have a state with energy E, which is the state with lowest energy, within $N+1$ randomly chosen states, distributed in energy according to $g_\mathrm{L}(E)$, is given by:

$$P(E) \propto \exp\left[-\beta_\mathrm{L}(E_0 - E)\right] \ \left[1 - \exp\left(-\beta_\mathrm{L}(E_0 - E)\right)\right]^N. \tag{3}$$

The previous expression corresponds to an asymmetric function that well reproduces the experimental spectra, in particular for a-Si:H [2] The observed red shift of the emission spectra with the decrease in the excitation energy was modeled by weighting equation (3) by an absorption factor $\alpha(E_\mathrm{x})$ that measures the probability to excite states with minimum energy E. The emission intensity, $I(E, E_\mathrm{x})$, was written as [2]:

$$I(E, E_x) \propto P(E)\ \frac{(E_x - E)^{\ 2}}{E_x}. \tag{4}$$

For $E_\mathrm{x} > E_0$, the emission spectra is independent of the excitation energy, while for $E_\mathrm{x} < E_0$ it is observed a red-shift of the emission peak energy with the decrease of the excitation energy. Equation (4) accurately reproduces the experimental data measured for the a-Si:H, suggesting a slope $m \approx 0.5$ for the linear region of the variation between E_p and E_x [2].

In order to evaluate the applicability of this model with respect to the experimental results concerning other a-SC, equation (4) was applied to fit the emission spectra of the d-U(2000) and d-U(600) di-ureasils, under different excitation energies. The fitting procedure was simultaneously applied to all the spectra minimizing the sum of the squared errors (Δ_1) between the calculated energy peak position and fwhm values using equation (4) and the measured ones. A good-quality fit was obtained and the resulting fit parameters, β_L, N, and E_0, together with the respective Δ_1 value are collected in Table 1. This procedure was also applied to a-Si:H. Similarly, the emission spectra of di-ureasils are well reproduced by equation (4) and the resulting fitting parameters are also listed in Table 1. The β_L, N, and E_0 listed in Table 1 obtained from the fit of the data for a-Si:H given by [4] are very close to the values reported by [2], namely $\beta_\mathrm{L} = 9.1\ \mathrm{eV}^{-1}$, $N = 50$, and $E_0 = 1.92$.

3.3 Model of thermal relaxation within localized states

Whilst the model proposed by Boulitrop et al. [2] explain qualitatively and quantitatively the experimental results,

Table 1. $\beta_{\rm L}$, E_0 and N parameters calculated from the fit of equation (5) to the emission spectra of d-U(2000), d-U(600), and a-Si:H recorded under different excitation energies. The fit error is also presented (Δ_1).

	E_0 (eV)	$\beta_{\rm L}$ (eV^{-1})	N	Δ_1 (eV)
a-Si:H	1.92	7.10	45	0.05
d-U(2000)	3.87	5.44	59	0.20
d-U(600)	3.74	6.44	56	0.15

the physical dynamic mechanisms behind the thermalization process in the localized states are not explicitly included. In an attempt to consider plainly these dynamic processes, we consider a thermal relaxation model within localized states. After the excitation of the electrons to high-energy states in the conduction band, there is relaxation to the bottom of the band where states are localized. At lower excitation energies it is also possible to excite directly to localized states. Due to the decrease of the density of states and the increase in their localization as we go to lower energies, thermalization of the electrons occurs in an increasingly higher time scale. During the thermalization within localized states we will assume that the electron can move accordingly to the extended multiple trapping model [5–7]. This means that the electron can move both to the conduction band and to localized states with higher and lower energy. Simultaneously to these transitions among localized states, radiative transitions may also occur. In the extended multiple trapping model, the transition rate, $t_{\rm ij}$, between two states with energy $E_{\rm i}$ and $E_{\rm j}$, whose localized wave function is centered around $\vec{r}_{\rm i}$ and $\vec{r}_{\rm j}$, respectively, is [6]:

$$t_{\rm ij}\left(|\vec{r}_{\rm ij}|\right) = f\left(E_{\rm i}, E_{\rm j}, T\right) P_{\rm ij}\left(|\vec{r}_{\rm ij}|\right), \tag{5}$$

where $|\vec{r}_{\rm ij}| = |\vec{r}_{\rm i} - \vec{r}_{\rm j}|$, $f\left(E_{\rm i}, E_{\rm j}, T\right)$ is a thermal activation factor and $P_{\rm ij}\left(|\vec{r}_{\rm ij}|\right)$ is the square of the transition matrix element [6]. The transition probability between the two states i and j depends on the overlap between the respective wavefunctions and, consequently, on the $r_{\rm ij}$ distance between the two states, and also on the characteristic reciprocal localization radius, $\lambda_{\rm i}$ and $\lambda_{\rm j}$. We will average over the position of the state j, considering a uniform distribution for the position of states through the sample. As proposed by Maschke et al., the average transition rate, $\bar{t}_{\rm ij}$, for an electron placed in $\vec{r}_{\rm i}$, with energy in the interval i, $[E_{\rm i} - \delta E/2, E_{\rm i} + \delta E/2]$, that moves to another state, whose energy belongs to the interval j, $[E_{\rm j} - \delta E/2, E_{\rm j} + \delta E/2]$, can be written as [6]:

$$\bar{t}_{\rm ij} = D\ f\ \left(E_{\rm i}, E_{\rm j}, T\right)\ h\left(\lambda_{\rm i}/\lambda_0, \lambda_{\rm j}/\lambda_0\right)\ g_{\rm L}\left(E_{\rm j}\right)\ \delta E, \tag{6}$$

where $g_{\rm L}\left(E_{\rm j}\right)\delta E_{\rm j}$ represents the concentration of localized electronic states in the conduction band tail states in the interval j and the expression for $h\left(\lambda_{\rm i}, \lambda_{\rm j}\right)$ can be found in reference [6]. Maschke and co-workers [6] estimated the prefactor D of the order of $10^{-6}\ \lambda_0^{-3}{\rm s}^{-1}$ for a-Si:H being λ_0 the reciprocal localization length for $E_{\rm j} = 0$. All the fits were made, taken $\delta E = 0.01$ eV.

The time dependence of the number of carriers that are in the energetic interval i, $n_{\rm i}$, and the number of carriers in the conduction band, n_0, are described by the following rate equation [6]:

$$\frac{{\rm d}n_{\rm i}}{{\rm d}t} = -n_{\rm i}\sum_{\rm j\neq i}\bar{t}_{\rm ij} + \sum_{\rm j\neq i} n_{\rm j}\bar{t}_{\rm ji} - \frac{n_{\rm i}}{\tau_{\rm i}}. \tag{7}$$

The first term represents the rate of carriers' loss, due to transitions to other states, and the second term denotes gains, due to transitions from other states. The third term corresponds to the radiative and non-radiative transitions. The parameter $\tau_{\rm i}^{-1} = \tau_{\rm i,r}^{-1} + \tau_{\rm i,nr}^{-1}$ is the sum of the radiative and non-radiative inverse transition rates. We are only interested in the total emission intensity with energy $E_{\rm i}$. This corresponds to the integrated intensity over time, after excitation of the system at $t = 0$ s.

The initial distribution of electrons $n_{\rm i}(0)$ generated by the excitation pulse depends on the excitation energy and is determined by the convolution of the density of states, according to:

$$n_0\left(0\right) \propto \begin{cases} \int\limits_{E_0<E<E_{\rm x}} g_{\rm c}\left(E\right) g_{\rm v}\left(E - E_{\rm x}\right)\ dE & \Leftarrow E_{\rm x} > E_0 \\ 0 & \Leftarrow E_{\rm x} < E_0 \end{cases} \tag{8}$$

$$n_{\rm i}\left(0\right) \propto \begin{cases} g_{\rm L}\left(E_{\rm i}\right) g_{\rm v}\left(E_{\rm i} - E_{\rm x}\right)\ \Delta E & \Leftarrow E_{\rm x} > E_{\rm i} \\ 0 & \Leftarrow E_{\rm x} < E_{\rm i}. \end{cases} \tag{9}$$

where $g_{\rm c}\left(E\right)$ is a parabolic density of states in the conduction band (for $E > E_0$),

$$g_c\left(E\right) = A_c\sqrt{E - E_0} \tag{10}$$

and $g_v\left(E\right)$ is a parabolic density of states in the valence band

$$g_\nu\left(E\right) = A_v\sqrt{-E} \tag{11}$$

where $A_{\rm c}$ and $A_{\rm v}$ are constants, that for simplicity are taken to be equal to each other and equal to A. The quantity $g_{\rm L}(E)$ is the localized band-tail of the conduction band given by

$$g_L\left(E\right) = C\exp\left[\beta\left(E - E_0\right)\right]. \tag{12}$$

Through the $\tilde{n}_{\rm i}\left(s\right)$ Laplace transform, the equation (7) is converted into a set of linear equations for each value of the variable s

The integrated intensity over time can be written as:

$$I\left(E_{\rm i}\right) = \int_0^\infty \frac{n_{\rm i}\left(t\right)}{\tau_{\rm r}}\,{\rm d}t = \frac{\tilde{n}_{\rm i}\left(0\right)}{\tau_{\rm r}}.$$

Since we are only interested in this quantity we only have to solve a system of linear equations to get $\tilde{n}_{\rm i}\left(0\right)$. To study the system under continuous excitation another term ($\gamma_{\rm i}$) should be added to equation (7), where $\gamma_{\rm i}$ represents the carriers generation rates for an energy state i created under continuous excitation. Under low excitation intensity

conditions this rate of carrier generation should be proportional to the initial distribution of carriers generated by an excitation pulse, i.e., $\gamma_i \propto n_i(0)$. Furthermore, the transition rates for low occupation of the states are exactly the same as before. In steady state, $\frac{\mathrm{d}n_i}{\mathrm{dt}} = 0$, and the rate equations reduce precisely to the same system of equations that, in this case, gives us the steady state occupation of each state, n_i, thus providing the steady state emission intensity, $I(E_i) = \frac{n_i}{\tau_{i,r}}$. Therefore, if the excitation intensity is low there is no difference in the integrated intensity after a pulsed excitation of the system at $t = 0$ s and the steady state regime.

In order to study the previous model, the following assumptions were made:

i) The reciprocal localization wavelength of the states close to the limits of the conduction band depends on the energy accordingly to [7]:

$$\lambda = \lambda_0 \left[1 - b\,(E - E_0)\right], \tag{13}$$

where λ_0 and b are constants [6];

ii) The radiative and non-radiative recombination decay times, τ_r and τ_nr, respectively, are independent of the energy of each state. We will consider an effective average decay time, τ_0, written as $\tau_0^{-1} = \tau_\mathrm{r}^{-1} + \tau_\mathrm{nr}^{-1}$;

iii) The electron, independently of the initial state, will recombine with a hole emitting energy (E_i–ΔE), where ΔE represents a certain constant energetic shift.

The constant shift ΔE can have several different physical origins — as in [6] we can argue that radiative recombination occurs at recombination centers at a constant energy in the gap. Shah et al. [4] proposed for a-Si:H that radiative recombination occurs between band tail electrons and self-trapped holes at localized band tail states having a well defined energy.

3.4 Fit results for the thermal relaxation model

The previous model was applied to a-Si:H, d-U(2000) and d-U(600). The fitting parameters of the model are: β, b, D, τ_0, E_0, together with the C and A of the density of states. The initial distribution of the excited carriers depends upon these two constants. This dependence occurs only for excitation energies higher than E_0. In order to keep the fitting as simple as possible we decided to keep these two parameters constant through all the fits reported and equal to the values $C = 10^{21}$ eV^{-1} cm^{-3} and $A = 6 \times 10^{21}$ eV$^{-3/2}$ cm^{-3} which are order of magnitude estimates for a-Si:H [3,4].

The constant C appears in the expression for the transition rates (Eq. (6)) as a product with the variable D and, consequently, only the product of these two constants, CD, can be obtained from the fit.

Considering that we have six fitting parameters and that many spurious local minima of the χ^2 error could occur we decided to use a genetic algorithm optimization package known to be able to search for global minima over rough error landscapes [24].

Table 2. Values of the interval of variation of the parameters used in fits for the thermal relaxation within localized states model.

β (eV^{-1})	CD (s^{-1} eV^{-1})	b (eV^{-1})	τ_0 (s^{-1})	ΔE (eV)	E_0 (eV)
[1, 20]	[10^{-8}, 10^{2}]	[0, 5000]	[10^{-5}, 10^{-2}]	[0, 0.5]	[1, 5]

The optimization algorithm requires that we start to define the intervals of variation for the parameters. The chosen intervals, for each fitting parameter, are listed in Table 2 and they are always the same for every one of the systems studied. We have chosen very broad variation intervals in order not to introduce any bias in the final value of the parameters. The fitting procedure was simultaneously applied to all the emission spectra available for each material. The optimization variable was the χ^2 error in the emission energy peak values, measured under different excitation energies.

The optimal fit parameters are listed in Table 3. A good quality fit was obtained for the samples as Figures 3a, 3b, and Figure 4 exemplify for the di-ureasils, and a-Si:H, respectively.

Comparing the values for β and E_0 in Table 1 with those found in Table 3 for a-Si:H, we realize that the values predicted by the model of thermal relaxation within localized states are similar to the ones suggested by the Boulitrop et al. model which are in the range $\beta = 6.7$–10 eV^{-1}. We should stress that the values of β given by this model are approximately equal to half the β values for the band tails (under the hypothesis of symmetric band-tails). For a-Si:H it is known that the experimental β for the valence band tail obtained from photoemission yield spectroscopy are in the range 12–20 eV^{-1} [2] depending on sample preparation. Experimental results for the conduction band tail give a higher β in the range 30–50 eV^{-1}. In [6] Maschke et al. used for the conduction band tail the value $\beta = 52.6$ eV^{-1}. Our β value for a-Si:H obtained using the steady state emission data of [3] and [4] is smaller and closer to the known values for the valence band-tail. The value obtained by us was a result of a fitting procedure to the emission peak shift as function of the excitation energy and should be regarded as an effective value that could be improved in several ways: (a) by extending the model considering both the energy dependence of the reciprocal lifetime of the carriers (b) by taking into account the effect of the hole energy distribution. (b) by including in the fitting procedure the width of the emission spectra.

The fitted E_0 parameter has a higher value for d-U(600), when compared with that determined for d-U(2000). Although the energy gap has not been experimentally measured by absorption measurements, several other arguments point out that d-U(2000) should have a smaller E_0 value. The size of the siliceous domains for each hybrid were previously determined by small-angle X-ray scattering, revealing that the siliceous domains in the d-U(600) are smaller than those present in the d-U(2000) di-ureasil, 4.0 and 5.2 Å, respectively [19,21]. In fact, in

Table 3. Values of the parameters β , CD, b, τ_0, $\Delta E$and E_0 obtained from the fit of the thermal relaxation within localized states model to the d-U(2000), d-U(600), and a-Si:H data. The fit χ^2 error is also presented.

	β (eV^{-1})	b (10^4 eV^{-1})	τ_0 (10^{-4} s)	ΔE (eV)	E_0 (eV)	CD (10^{16} s eV^{-1})	χ^2 ($10^{-4}eV^2$)
a-Si:H	12.08	1.50	9.9	0.244	1.896	9.56	2.8
d-U(2000)	4.36	0.938	3.96	0.213	3.622	1.49	20.2
d-U(600)	5.08	1.15	69.5	0.211	3.882	2.56	54.8

silicon-based nanostructured materials the dimensional hierarchy of the backbone determines the energy, in such a way that an increase in the siliceous network corresponds to a decrease in the respective energy gap [25]. In accordance with that, a higher E_0 values could be expected for the d-U(600) di-ureasil.

The lifetime τ_0 was considered independent of the energy of each state, assumption ii) in Section 3.3. The consequence of this assumption is that the predicted emission decay is described by a single exponential function. However, it is often reported non-exponential decay curves for amorphous and disordered materials. In such case, the reciprocal lifetime τ_0^{-1} should be taken as dependent on the energy of the initial states $\tau_0^{-1}(E)$. For the particular case of a-Si:H, the energy dependent τ_0 values considered by Maschke et al. [6] approximately varies between 10^{-6} to 10^{-1} s. Comparing this interval range with the effective lifetime using the model of thermal relaxation within localized states ($\sim 1\times10^{-3}$ s, see Tab. 3) we verify that the fitted τ_0 value is within the interval and thus should be regarded as an effective lifetime consistent with the value obtained by Maschke et al. [6]. Furthermore, the energy dependent consideration, $\tau_0(E)$, introduces a number of additional fitting parameters, thus increasing the complexity of the fit and requiring a detailed time-dependent experimental data, that go beyond the main goal of this work.

On the contrary, the decay curves of the di-ureasils are well reproduced by single exponential functions [20,21], supporting the assumption of an energy independent effective lifetime. Furthermore, the τ_0 value obtained from our fitting procedure to the steady-state emission spectra are of the order of the millisecond (Tab. 3) as it is the case for the lifetime values, $3.5 \pm 0.1 \times 10^{-3}$ and $4.7 \pm 0.1 \times 10^{-3}$ s, experimentally determined for d-U(2000) and d-U(600), respectively [20].

To study the sensibility and stability of our model, the input parameters were modified, namely, the reciprocal localization wavelength of the states λ was considered as energy independent ($b = 0$, in Eq. (14)). Such assumption lead to poor quality fits and induces major changes in E_0 and τ_0. In both cases, higher values were found for E_0, which are not supported by experimental results, and τ_0 decreased to $\approx 10^{-7}$–10^{-9} s, which is an abnormal small value accordingly to previous estimations for a-Si:H [6]. We have also made fits considering $\Delta E = 0$ that gave smaller β values and slightly larger E_0 values that were not consistent with independent estimations available for a-Si:H [2–4].

4 Conclusion

In this work we studied the emission red-shift as the excitation energy decreases, in some amorphous semiconductors. Emphasis was given to organic/inorganic di-ureasils, previously studied by some of us, which have promising applications as novel photonic hybrid materials. Despite the experimental work done in recent years in these multifunctional hybrids, their emission features have been only qualitatively discussed. Here we proposed a new model of thermal relaxation within localized states, in the framework of the extended multiple trapping approach, to describe those emission properties. The fitted E_0 and β_L values obtained using the thermal relaxation within localized states representation are consistent with those obtained using the Boulitrop's model [2]. However, because we explicitly consider the energy dependence of the electron transfer rates between localized states in competition with radiative and non-radiative decay times; our description is more physically detailed. Furthermore, the model proposed here can be used to study simultaneously time-dependent and steady-state emission (absent in the previous studies of the emission red-shift as the excitation energy decreases) and thus the same fitting values of the parameters should be able to describe both phenomena.

The financial support from FEDER and Fundação para a Ciência e a Tecnologia, POCT and POCI programs (CTM/46780/02, CTM/59075/2004 and BD/18404/98), is gratefully acknowledged.

References

1. (a) 1989 *Amorphous Insulators and Semiconductors*, edited by M.F. Thorpe, M.I. Mitkova (Kluwer Academic Publishers); (b) G.J. Adriaenssens, in *Amorphous Insulators and Semiconductors*, edited by M.F. Thorpe, M.I. Mitkova (Kluwer Academic Publishers, 1989) pp. 437–468
2. F. Boulitrop, D.J. Dunstan, Phys. Rev. B **28**, 5923 (1983); D.J. Dunstan, F. Boulitrop. Phys. Rev. B **30**, 5945 (1984)
3. W.-C. Chen, B.J. Feldman, J. Bajaj, F.-M. Tong, G.K. Wong, Solid State Commun. **38**, 357 (1981)
4. J . Shah, A. Pinczuk, F.B. Alexander, B.G. Bagley, Solid State Commun. **42**, 717 (1982)
5. K. Maschke, E. Merk, W. Czaja, J. Non-Crist. Solids **77–78**, 687 (1985)
6. K. Maschke, E. Merk, W. Czaja, Phil. Mag. B **56**, 457 (1987)

7. W. Czaja, K. Maschke, E. Merk, J. Lumin. **40–41**, 559 (1988)
8. S.P. Depinna, B.C. Cavenett, W.E. Lamb, Phil. Mag. B **47**, 99 (1982)
9. R.C. Fang, J. Lumin. **48–49**, 631 (1991)
10. J. Rusli, J. Robertson, G.A. Amaratunga, J. Appl. Phys. **80**, 2998 (1996)
11. R. Fang, Y. Song, W. Jiang, K. Yan, J. Lumin. **40–41**, 905 (1988)
12. S.V. Chernvshov, E.I. Terukov, V.A. Vassilyev, A.S. Volkov, J. Non-Cryst. Solids **134**, 218 (1991)
13. V.P. Bondarenko, V.E. Borisenko, A.M. Dorofeev, I.N. Germanenko, S.V. Gaponenko, J. Appl. Phys. **75**, 2727 (1994)
14. I. Hirabayashi, K. Morigaki, S. Yamanaka, J. Non-Cryst. Solids **59–60**, 645 (1983)
15. (a) V. Bekiari, P. Lianos, Langmuir **14**, 3459 (1998); (b) V. Bekiari, P. Lianos, Chem. Mater. **10**, 3777 (1998)
16. V. de Zea Bermudez, L.D. Carlos, M.C. Duarte, M.M. Silva, C.J. Silva, M.J. Smith, M. Assunção, L. Alcácer, J. Alloys and Compounds **275–277**, 21 (1998)
17. S.J.L. Ribeiro, K. Dahmouche, C.A. Ribeiro, C.V. Santilli, S.H. Pulcinelli, J. Sol-Gel Sci. Tech. **13**, 427 (1998)
18. L.D. Carlos, R.A. Sá Ferreira, V. de Zea Bermudez, C. Molina, L.A. Bueno, S.J.L. Ribeiro, Phys. Rev. B **60**, 10042 (1999)
19. (a) L.D. Carlos, V. de Zea Bermudez, R.A. Sá Ferreira, L. Marques, M. Assunção, Chem. Mater. **11**, 581 (1999); (b) R.A. Sá Ferreira, L.D. Carlos, V. de Zea Bermudez, Thin Solid Films **343**, 476 (1999)
20. L.D. Carlos, R.A. Sá Ferreira, V. de Zea Bermudez, S.J.L. Ribeiro, Adv. Func. Mater. **2**, 111 (2001)
21. (a) L.D. Carlos, R.A. Sá Ferreira, V. de Zea Bermudez, *in Handbook of Organic-Inorganic Hybrid Materials and Nanocomposites*, edited by H.S. Nalwa (American Scientific Publishers, Morth Lewis Way, Califórnia) Vol. 1, Chap. 9, pp. 353–380; (b) L.D. Carlos, R.A. Sá Ferreira, R.N. Pereira, M. Assunção, V. de Zea Bermudez, J. Phys. Chem. B **108**, 14924 (2004)
22. *Functional Hybrid Materials*, edited by P.G. Romero, C. Sanchez (Wiley-VCH, Weinheim, 2003)
23. C. Sanchez, B. Julián, P. Belleville, M. Popall, J. Mat Chem. **15**, 3559 (2005)
24. *A Genetic Algorithm for Function Optimization: A Matlab Implementation* by C. Houck, J. Joines, M. Kay, NCSU-IE TR 95-09, 1995
25. (a) T. Takagahara, K. Takeda, Phys. Rev. B **46**, 15578 (1992); (b) G. Allan, C. Delerue, M. Lannoo, Phys. Rev. B **48**, 7951 (1993); (c) Y. Kanemitsu, K. Susuki, S. Kyushin, H. Matsumoto, Phys. Rev. B **51**, 13103 (1995); (d) A.O. Konstantinov, A. Henry, C.I. Harry, E. Janzén, Appl. Phys. Lett. **66**, 2250 (1995)